# Multiscale Modeling of Barium Sulfate Formation from BaO – Supporting Information

Nikola Rankovic,*,†,‡ Céline Chizallet,§ André Nicolle,* and Patrick Da Costa †

## 1 Detailed Parameters Used for Simulating BaO Surfaces

Table S.1: Parameters Used for the Simulation of BaO Surfaces and the Resulting Surface Energy After Relaxation. For Some Systems, a Reduction of the $k$-points Grid Was Necessary With HSE06 Hybrid Functional to Compensate Very Long Computational Times

| System | (100) Terrace | Monoatomic step | Kink |
|---|---|---|---|
| Number of atoms per supercell | 80 | 72 | 106 |
| Supercell size (Å) along the | | | |
| $x$-axis | 11.09 | 11.09 | 16.64 |
| $y$-axis | 11.09 | 8.77 | 8.77 |
| $z$-axis: slab thickness | 11.09 | 14.91 | 14.91 |
| $z$-axis: vacuum thickness | 17.00 | 19.00 | 19.00 |
| Projected surface area (Å$^2$) | 123.07 | 97.30 | 145.95 |
| $k$-points mesh | $3\times3\times1$ (GGA)<br>$2\times2\times1$ (HSE06) | $3\times2\times1$ (GGA)<br>$2\times2\times1$ (HSE06) | $1\times2\times1$ |
| Surface energy $\Gamma$ after relaxation (J m$^{-2}$) | 0.29 | 0.43 | 0.50 |

## 2 Investigation of the Surface Reconstruction Phenomena: Molecular Dynamics

Velocity-scaled molecular dynamics (MD) were performed each time a surface reconstruction phenomenon was encountered to explore the stability of the obtained geometry. Velocities were scaled at each time step (5 fs) to the chosen temperature (600 K). The calculation accuracy was decreased to limit computational cost to a cut-off energy of 300 eV and the convergence criterion for the electronic SCF loop was reduced to $1\times10^{-4}$ eV. The energetic minima obtained from MD simulations were quenched by 0 K geometry optimization with usual accuracy (see the "Computational Methods" section in the manuscript) and the most stable quenched structures are assumed to give the best estimate of the most energetically favorable configurations for each explored coverage value. The evolution of the potential energy as a function of time is given in Figure S.1.

*IFP Energies nouvelles, 1-4 avenue de Bois-Préau, 92852 Rueil-Malmaison Cedex, France

†Institut Jean Le Rond d'Alembert – Université Pierre et Marie Curie – UPMC Paris 6, CNRS-UMR 7190, 2 place de la gare de ceinture, 78210 Saint-Cyr-l'Ecole, France

‡New Address: Aramco Fuel Research Center, 232 Avenue Napoléon Bonaparte, 92500 Rueil-Malmaison, France

§IFP Energies nouvelles, établissement de Lyon, Rond-point de l'échangeur de Solaize, BP 3, 69360 Solaize, France

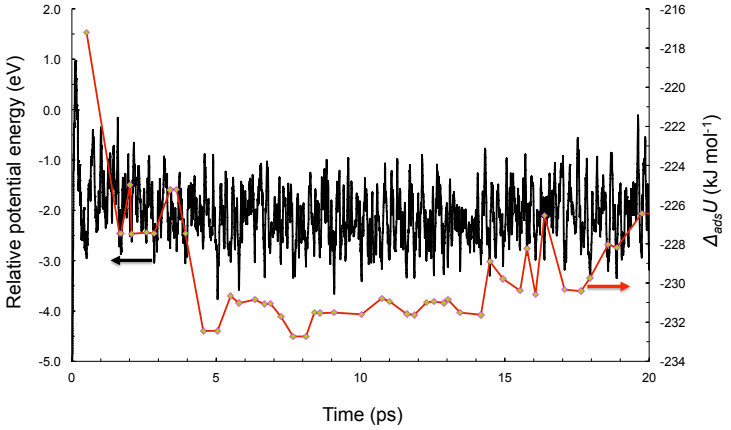


(a) BaO(100)–$SO_2$ at 0.5 ML

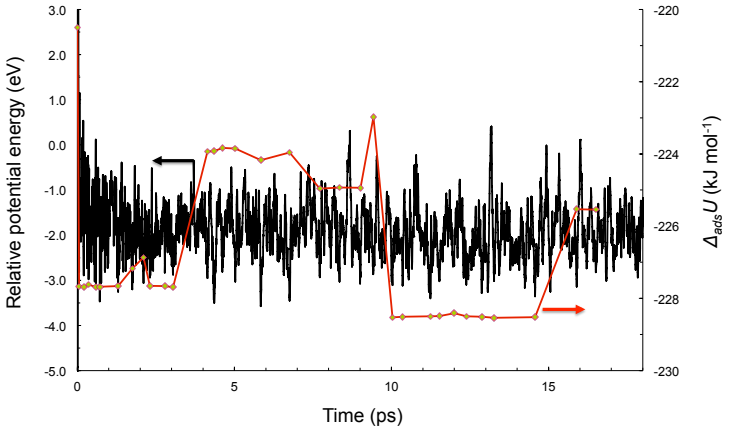


(b) BaO(100)–$SO_2$ at 0.75 ML

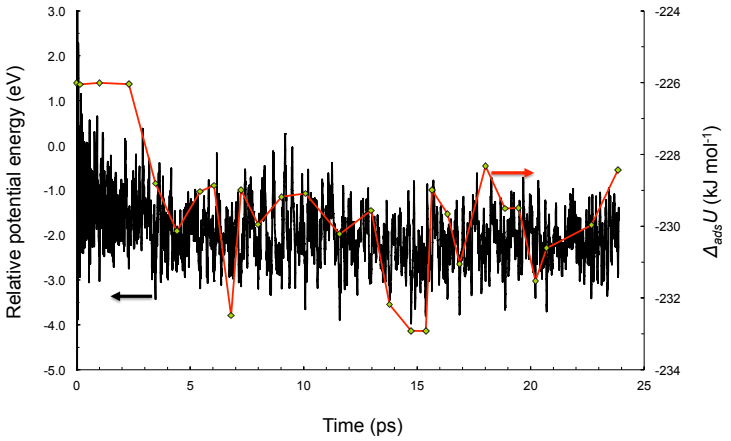


(c) BaO(100)–$SO_2$ at 1 ML

Figure S.1: Evolution of the potential energy relative to the initial geometry optimization during a 600 K MD simulation of $SO_2$ adsorbed on BaO(100) terrace at (a) 0.5 ML, (b) 0.75 ML and (c) 1 ML fractional coverage (black). Energetic minima were further quenched and their energies calculated at the GGA level are also reported (red).

# 3 Activation Barriers for SO$x$ Adsorption on BaO(100)

Some additional investigations of SO$x$ adsorption on BaO aimed to provide an insight into the adsorption kinetics. This was achieved by tracing the energetic profile of a SO$x$ molecule approaching a basic $O_{5C}$ site (calculations performed at the GGA level). For this purpose, the most stable structure obtained for the adsorption on a BaO(100) terrace was distorted by increasingly moving the molecule away from the surface along the $z$ axis and keeping the $O_{5C}$–S distance fixed while allowing all other atoms to relax. The adsorption energy profile of the $SO_3$ molecule (Figure S.2) illustrates a transition from a physisorbed to a chimisorbed state. No noticeable activation barrier for a transition from the gas-phase $SO_3$ to a chimisorbed state was observed for this perpendicular approach. This finding is particularly interesting for the conception of the kinetic model, allowing us to postulate a non-activated surface $SO_3$ adsorption.

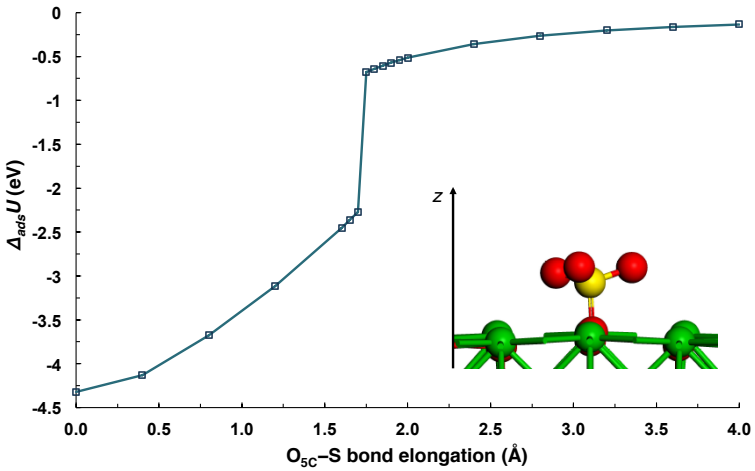


Figure S.2: $SO_3$ molecule adsorbed onto a basic oxygen site of the BaO surface. Energetic profile for the $SO_3$–BaO(100) system as the molecule approaches the basic surface site along the $z$ axis. The bond elongation is relative to the equilibrium bond length of 1.57 Å.

According to the adsorption energy profile for the $SO_2$ molecule (Figure S.3), we can see that no significant activation barrier seems to exist to reach the final chimisorbed state from the gas phase, along a perpendicular approach. The existence of a shallow precursor state (denoted by a star on Figure S.3) will have to be confirmed in the future work. We thus postulate, similarly to the case of $SO_3$ adsorption, a non-activated adsorption process for $SO_2$ in first approximation.

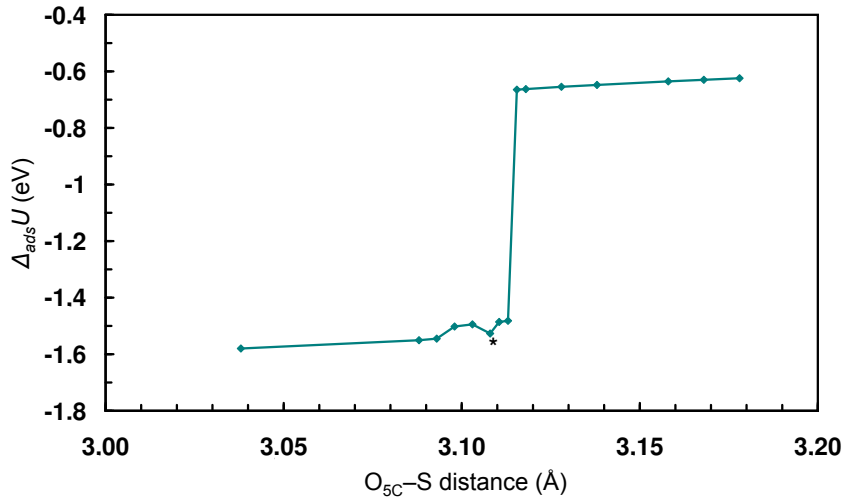


Figure S.3: The energetic profile of the $SO_2$–BaO(100) system as a function of the $O_{5C}$–S distance.

# 4 Extrapolation of the Adsorption Energies over the 0–1 ML range

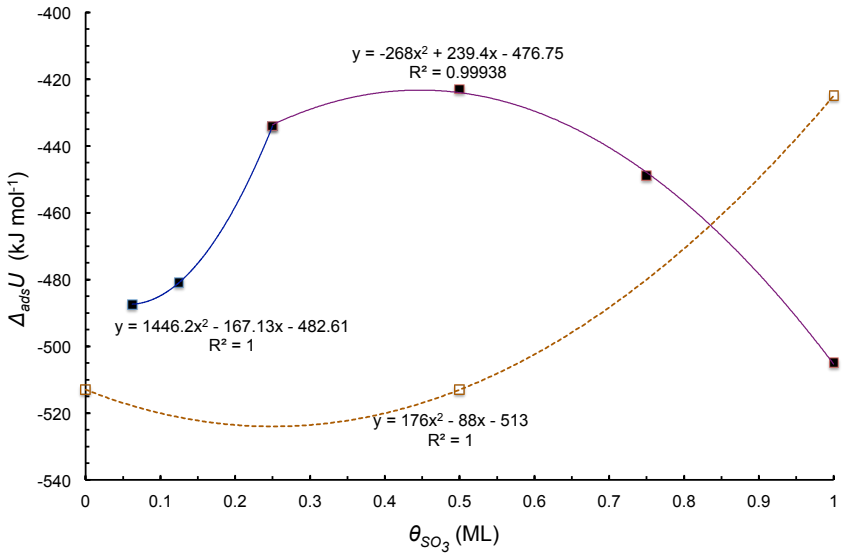


(a)

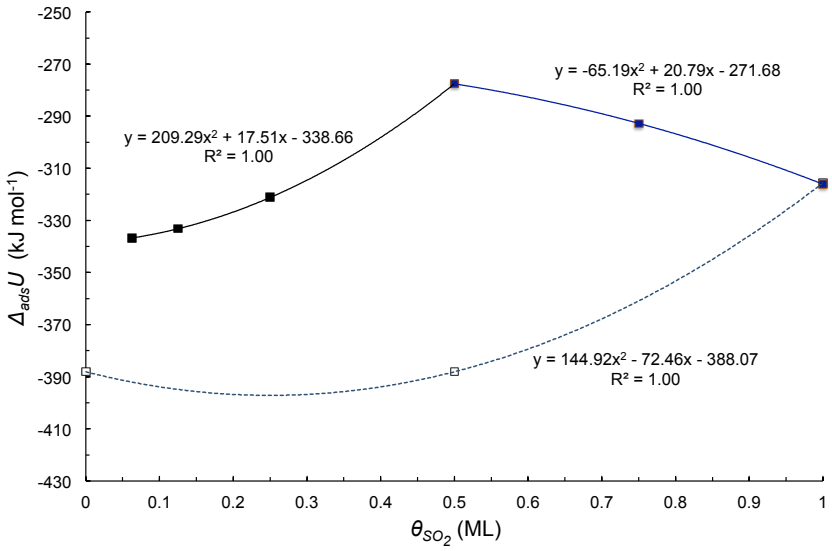


(b)

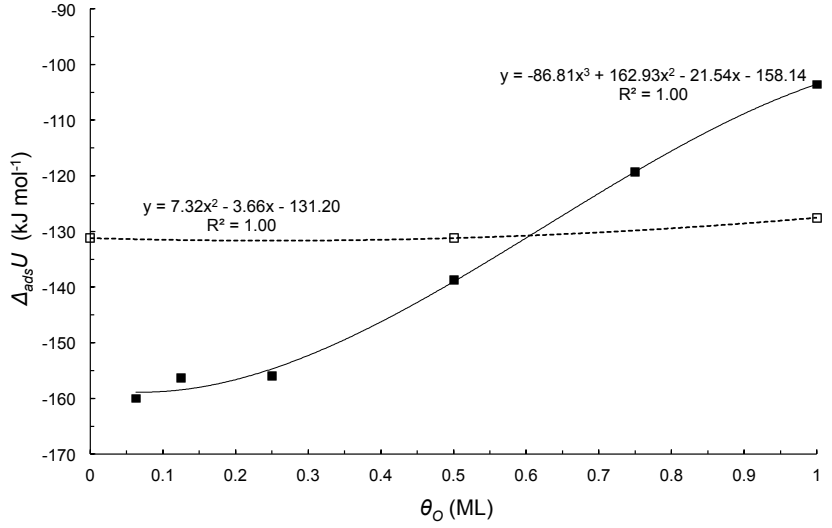


(c)

Figure S.4: Polynomial extrapolation of $SO_3$, $SO_2$, and $O_2$ adsorption energies on BaO(100) terraces (filled symbols, solid lines) and on surface steps (open symbols, dashed line) over the 0–1 ML coverage range.

# 5 Kinetic and Thermodynamic Parameters Used for Kinetic Modeling

Table S.2: Kinetic and Thermodynamic Parameters Used for Kinetic Modeling of Reactions $R1$–$R14$

| Reaction | $A$ ($s^{-1}$) | $Ea$ (kJ $mol^{-1}$) | $\Delta rU$ (kJ $mol^{-1}$) | $\Delta rS$ (J $mol^{-1}$ $K^{-1}$) |
|---|---|---|---|---|
| *R1* | $1.00 \times 10^6$ | 0.0 | $209.29 \times \theta_{SO_2}^2 - 17.51 \times \theta_{SO_2} - 338.66$ for $\theta_{SO_2} \leq 0.5$ ML and $-65.19 \times \theta_{SO_2}^2 + 20.79 \times \theta_{SO_2} - 271.68$ for 0.5 ML $< \theta_{SO_2} \leq 1$ ML | -251 |
| *R2* | $1.00 \times 10^6$ | 0.0 | $144.92 \times \theta_{SO_2}^2 - 72.46 \times \theta_{SO_2} - 388.07$ | -251 |
| *R3* | $1.00 \times 10^6$ | 0.0 | -408 | -251 |
| *R4* | $1.63 \times 10^4$ | 68.6 | $-86.81 \times \theta_O^3 + 162.93 \times \theta_O^2$ $-21.54 \times \theta_O - 158.14$ | -152 |
| *R5* | $1.63 \times 10^4$ | 68.6 | $7.32 \times \theta_O^2 - 3.66 \times \theta_O - 131.20$ | -152 |
| *R6* | $1.63 \times 10^4$ | 68.6 | -123 | -152 |
| *R7* | $1.63 \times 10^4$ | 68.6 | -127 | -202 |
| *R8* | $1.00 \times 10^{13}$ | 20.0 | -70 | -19 |
| *R9* | $1.00 \times 10^{13}$ | 20.0 | -50 | -19 |
| *R10* | $1.00 \times 10^{13}$ | 20.0 | -61 | -19 |
| *R11* | $1.00 \times 10^6$ | 0.0 | $1446.20 \times \theta_{SO_3}^2 - 167.13 \times \theta_{SO_3} - 482.16$ for $\theta_{SO_3} \leq 0.5$ ML and $-268.00 \times \theta_{SO_3}^2 + 239.40 \times \theta_{SO_3} - 476.75$ for 0.5 ML $< \theta_{SO_3} \leq 1$ ML | -246 |
| *R12* | $1.00 \times 10^6$ | 0.0 | $176 \times \theta_{SO_3}^2 - 88 \times \theta_{SO_3} - 513$ | -246 |
| *R13* | $1.00 \times 10^6$ | 0.0 | -531 | -246 |
| *R14* | $1.00 \times 10^7$ | 80.5 | -505 | -314 |

# 6 Storage mechanism analysis

Additional information about storage mechanisms is provided herein.

Figures S5(a) and S5(b) provide rate analysis for the case of $SO_2$ and $SO_3$ storage, respectively. Note that all rate values in Figure S5(b) represent net reaction rates ($r_{forward} - r_{backward}$), thus negative numerical values suggest backward processes taking over forward ones ($SO_2$ desorption and $SO_3$ decomposition).

Figures S6(a) and S6(b) provide surface coverage evolution during $SO_2$ and $O_2$ coadsorption simulation.

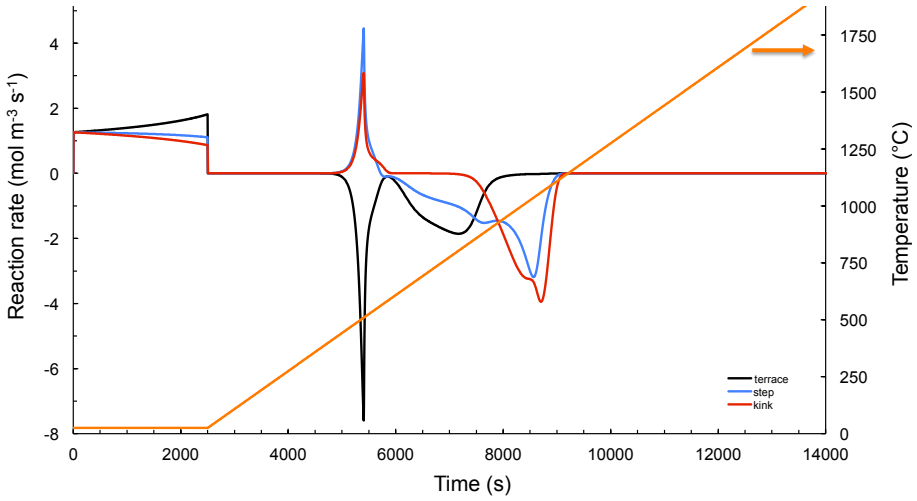


(a)

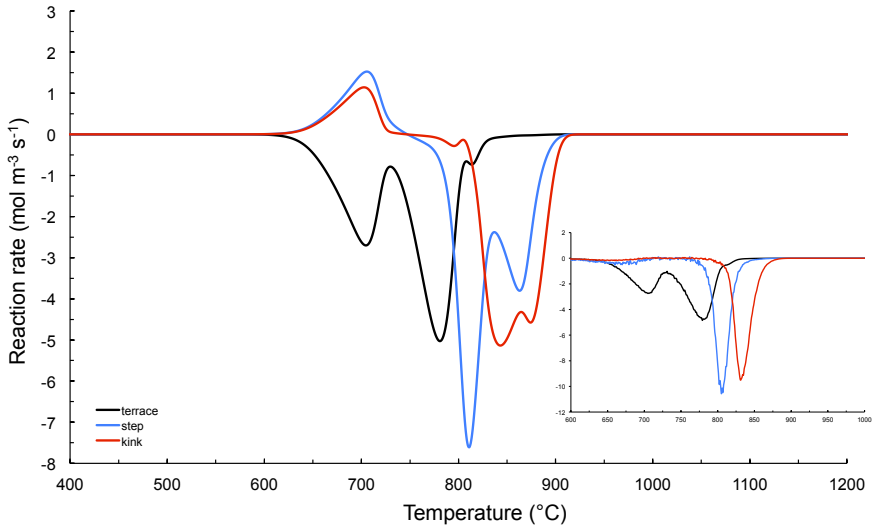


(b)

Figure S.5: (a) Analysis of the $SO_2$ storage–TPD simulation: net reaction rates versus time. The $SO_2$ storage phase ends at 2500 s. For illustration purposes, temperature profile is also given (orange). (b) Analysis of $SO_3$ storage. Storage phase: 200 ppm $SO_3$ in He at 25°C during 2500 s. Net $SO_2$ adsorption rates versus temperature. Inset: net $SO_2$ oxidation rates on BaO (opposite of $SO_3$ to $SO_2$ reduction rate).

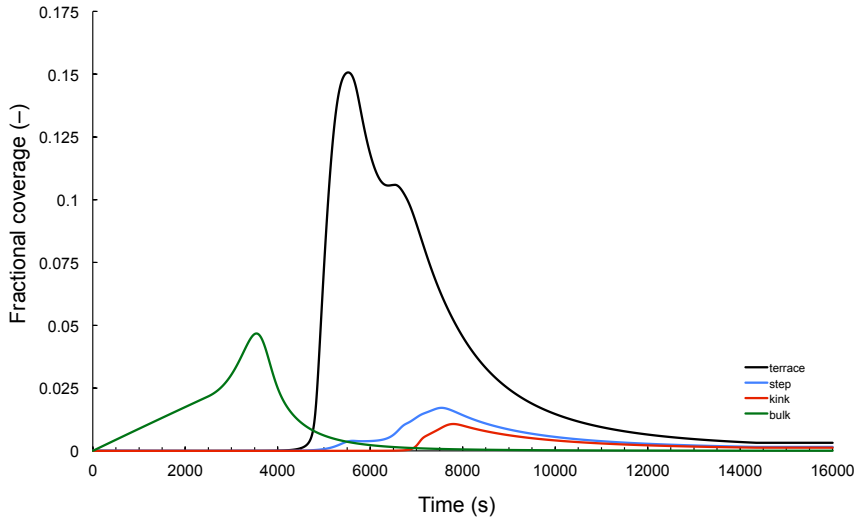


(a)

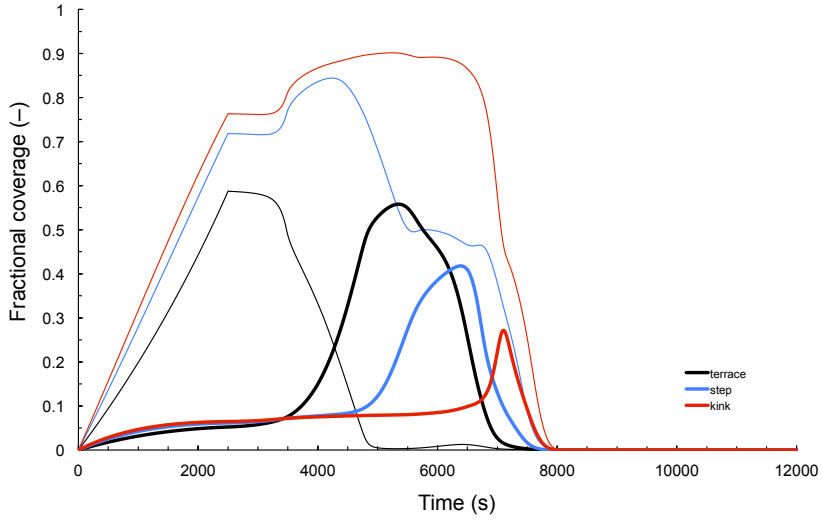


(b)

Figure S.6: Analysis of the 200 ppm $SO_2$ + 21 vol. % $O_2$ coadsorption simulation. (a) Barium peroxide fractional coverage; (b) $SO_3$ (thick lines) and $SO_2$ (thin lines) fractional coverages.